

Non-aligned MHD stagnation-point flow of upper-convected Maxwell fluid with nonlinear thermal radiation

M. Mustafa¹ · A. Mushtaq² · T. Hayat^{3,4} · A. Alsaedi⁴

Received: 17 February 2016 / Accepted: 23 November 2016 / Published online: 18 December 2016
© The Natural Computing Applications Forum 2016

Abstract Present analysis is performed for non-aligned stagnation-point flow of upper-convected Maxwell fluid over a continuously deforming surface. Aspects of nonlinear radiation flux and heat source/sink are invoked in the thermal analysis. Self-similar differential system is formulated by means of similarity transformations. Numerical computations for velocity and temperature profiles are made through standard shooting approach with fifth-order Runge–Kutta method. A collocation method-based MATLAB package *bvp4c* is also implemented for finding solutions. The results show that velocity and temperature profiles are appreciably affected when the viscoelastic fluid parameter is varied. The inclusion of radiation flux term yields an additional parameter (θ_w) that is helpful for analysis of even large wall and ambient temperature differences. It is found that the concavity of the temperature function changes in its domain when sufficiently large wall-to-ambient temperature ratio is imposed. A comparative study about linear and nonlinear radiative heat fluxes

is also presented. The results agree very well with the results of an existing article in a special situation.

Keywords Non-aligned stagnation point · Maxwell fluid · Numerical method · Viscoelastic fluid · Heat transfer

1 Introduction

Many liquids of engineering importance have nonlinear relationship between stress and shear rate, and hence, their flow behavior cannot be predicted through the usual Newton's law of viscosity. Some examples of these fluids are molten plastics, gelatin, polymers, dyes, paints, bloods, multi-grade oils, shampoos, fruit juices and honey. An important characteristic of these fluids is the retention of a fading memory of their flow history, which is termed as elasticity. Apart from viscosity, the viscoelastic fluids exhibit normal stress effects attributed to the fluid elasticity. These fluids have certain amount of energy stored in the form of strain energy which is responsible for the partial elastic recovery upon the removal of stress. One of the popular models of viscoelastic fluids is the upper-convected Maxwell (UCM) fluid model which explains the influence of fluid memory in view of the fluid relaxation time. In the past, the boundary layer flows of UCM fluid have been given special attention by the research community. For instance, Sadeghy et al. [1] investigated the two-dimensional flow of Maxwell fluid over a flat plate in a calm fluid. They discussed a comparative study of different numerical and analytical approaches for solving the developed nonlinear problem. Later, Kumari and Nath [2] analyzed buoyancy effects on Maxwell fluid flow in the region of stagnation point. They developed numerical approximations by finite difference method and observed that fluid velocity near the

✉ M. Mustafa
meraj_mm@hotmail.com

¹ School of Natural Sciences (SNS), National University of Sciences and Technology (NUST), Islamabad 44000, Pakistan

² Research Centre for Modeling and Simulation (RCMS), National University of Sciences and Technology (NUST), Islamabad 44000, Pakistan

³ Department of Mathematics, Quaid-I-Azam University, 45320, Islamabad 44000, Pakistan

⁴ Nonlinear Analysis and Applied Mathematics (NAAM) Research Group, Department of Mathematics, Faculty of Science, King Abdulaziz University, Jeddah 21589, Saudi Arabia

plate has inverse relation with the viscoelastic fluid parameter. Abel et al. [3] examined the Maxwell fluid flow adjacent to a stretchable surface utilizing a numerical technique. Hayat et al. [4] analyzed melting effects in Maxwell fluid flow near a stagnation point on a deforming surface. Shateyi [5] introduced a numerical method for tackling the Maxwell fluid flow with mass transfer. Recently, several interesting contributions regarding the flow analysis of Maxwell fluid are made [6–14].

Radiative heat transfer has special significance in engineering processes such as solar power technology, nuclear power plant, satellites and space vehicles; in combustion applications such as fires, furnaces, IC engines; and in solar radiation buildings. The concept of nonlinear radiation flux for laminar flow was first introduced by Rahman and El-tayeb [15]. They considered the nanofluid flow due to nonlinearly deforming surface using nonlinear Rosseland heat flux. Pantokratoras and Fang [16] examined heat transfer mechanism for laminar flow past a constantly moving radiative plate utilizing nonlinear radiative flux term. In another paper, Pantokratoras and Fang [17] analyzed the well-known Blasius flow subject to nonlinear radiation flux. Stagnation-point flow of Maxwell fluid subject to nonlinear thermal radiation was investigated by Mushtaq et al. [18]. Cortell [19] analyzed onset of the nonlinear radiation flux effects flow developed by quadratic deforming surface. Recently, various researchers discussed the nonlinear radiation flux aspect under different situations [20–25].

Here, our main objective is to discuss the non-aligned stagnation-point flow of an electrically conducting Maxwell fluid past a stretchable boundary considering nonlinear thermal radiation and heat source effects. The present study is an extension of the work reported by Abel et al. [3]. The present attempt is important to determine the onset of viscoelasticity and magnetic field on the heat transfer rate which is of fundamental interest in many extrusion processes. In recent past, some interesting numerical/analytical approaches for tackling MHD boundary layer equations have been proposed [26–40]. In the next section, we present the problem formulation. Section 3 deals with the description of numerical method and results. In Sect. 4, the conclusions of the present work are reported.

2 Basic equations

Consider a Maxwell fluid flow past a stretchable surface residing along the x -axis. Let the flow far from the sheet be characterized by $u = bx$, $v = -by$, where b denotes the intensity of the stagnation flow. The velocity components at the surface are $u = a(x + c)$, $v = 0$, where $a > 0$ denotes the rate of stretching and c indicates the point of stretching origin. It means that the axis of stretching and

the free stream are not aligned in general. Magnetic field with uniform strength B_0 acts normal to the stretching boundary, and induced magnetic field is ignored by assuming low magnetic Reynolds number. Let T_w be the constant temperature of the stretching boundary which is assumed to be larger than ambient temperature T_∞ . Relevant equations which govern the laminar flow and radiative heat transfer of UCM fluid are expressed below [5, 25]:

$$\frac{\partial u}{\partial x} + \frac{\partial v}{\partial y} = 0, \quad (1)$$

$$u \frac{\partial u}{\partial x} + v \frac{\partial u}{\partial y} + \lambda_1 \left(u^2 \frac{\partial^2 u}{\partial x^2} + v^2 \frac{\partial^2 u}{\partial y^2} + 2uv \frac{\partial^2 u}{\partial x \partial y} \right) = U_\infty \frac{dU_\infty}{dx} + v \frac{\partial^2 u}{\partial y^2} - \frac{\sigma B_0^2}{\rho} \left(u - U_\infty + \lambda_1 v \frac{\partial u}{\partial y} \right), \quad (2)$$

$$u \frac{\partial T}{\partial x} + v \frac{\partial T}{\partial y} = \frac{\partial}{\partial y} \left(\alpha + \frac{16\sigma^*}{3\rho C_p k^*} T^3 \right) \frac{\partial T}{\partial y} + Q(T - T_\infty), \quad (3)$$

where the coordinate x extends along the surface and y is normal to it. u and v denote the fluid velocities in x - and y -directions, respectively, λ_1 is the fluid relaxation time, ν stands for kinematic viscosity, ρ represents the fluid density, σ denotes the fluid electrical conductivity, C_p is the specific heat capacity, σ^* and k^* denote the Stefan–Boltzmann constant and the mean absorption coefficient, respectively, and Q is heat source/sink parameter. The boundary conditions for problem under consideration are [40]:

$$\begin{aligned} u = U_w(x) = a(x + c), v = 0, T = T_w \quad \text{at } y = 0, \\ u = U_\infty(x) = bx, v = -by, T \rightarrow T_\infty \quad \text{as } y \rightarrow \infty. \end{aligned} \quad (4)$$

Consider the following transformations:

$$\eta = y \sqrt{\frac{a}{\nu}}, \quad u = axf'(\eta) + bch(\eta), \quad v = -\sqrt{a\nu}f(\eta). \quad (5)$$

Equation (1) is satisfied identically in view of (5). Making use of variables (5) in Eq. (2) and then equating like powers of x and x^0 , we arrive at the following coupled ordinary differential equations:

$$\begin{aligned} f''' - f'^2 + ff'' + De(2ff'f'' - f^2f''') + M(\gamma - f' + Deff'') \\ + \gamma^2 = 0, \end{aligned} \quad (6)$$

$$h'' + fh' - hf' + De(2hff'' - f^2h'') + M(Defh' - h) = 0. \quad (7)$$

In order to find similar form of Eq. (3), we define a non-dimensional temperature as $\theta(\eta) = (T - T_\infty)/(T_w - T_\infty)$. Thus, we have $T = T_\infty(1 + (\theta_w - 1)\theta)$, where $\theta_w = T_w/T_\infty$. So first term on the right-hand side of Eq. (3) can be written as $\alpha \frac{\partial}{\partial y} \left[1 + Rd(1 + (\theta_w - 1)\theta) \right]$ in which $Rd = 16\sigma^*T_\infty^3/3kk^*$ denotes the radiation parameter. This expression can be further reduced to $\frac{a(T_w - T_\infty)}{Pr} [1 + Rd(1 +$

$(\theta_w - 1)\theta^3 \theta']'$ where $Pr = \nu/\alpha$ denotes the Prandtl number. Equation (8) in non-dimensional form is given below:

$$\frac{1}{Pr} \left[\left(1 + Rd(1 + (\theta_w - 1)\theta^3) \right) \theta' \right]' + f\theta' + S\theta = 0. \tag{8}$$

In Eqs. (6)–(8), $De = \lambda_1 a$ is the viscoelastic fluid parameter (also referred to as Deborah number), $\gamma = b/a$ the stretching rates ratio, $S = Q/a$ the heat source/sink parameter, and $M = \sigma B_0^2/\rho a$ the magnetic field parameter. The transformed conditions are:

$$\begin{aligned} f(0) = 0, \quad f'(0) = 1, \quad h(0) = 1, \quad \theta(0) = 1, \\ f'(\infty) \rightarrow \gamma, \quad h(\infty) \rightarrow 0, \quad \theta(\infty) \rightarrow 0. \end{aligned} \tag{9}$$

Quantity of practical interest here is the local Nusselt number Nu_x defined as follows:

$$Nu_x = \frac{xq_w}{k(T_w - T_\infty)}, \tag{10}$$

where $q_w = -k(\partial T/\partial y)_{y=0} + (q_r)_{y=0}$ is the wall heat flux. Now using dimensionless quantities from Eq. (5) in Eq. (10), one obtains

$$Re_x^{-1/2} Nu_x = -[1 + Rd\theta_w^3] \theta'(0), \tag{11}$$

where $Re_x = U_w x/\nu$ is the local Reynolds number.

3 Numerical method

A standard shooting approach using fifth-order Runge–Kutta (RK5) method is implemented for finding approximations of the differential Eqs. (6)–(8) subject to the conditions (9). RK method is generally a preferred integration technique since it uses derivative information at the midpoint of stepping interval. It acquires advantages of faster convergence and simple implementation of the methods for initial value problems. Fifth-order refers to the magnitude of the error term in RK method. The present fifth-order RK method also works with adaptive step size which makes it computationally efficient than the usual Euler method or finite difference schemes. Substituting $y_1 = f, y_2 = f', y_3 = f'', y_4 = h, y_5 = h', y_6 = \theta, y_7 = \theta'$, we obtain first-order system comprising of seven ordinary differential equations given below:

$$\begin{aligned} y_1' &= y_2; \quad y_1(0) = 0 \\ y_2' &= y_3; \quad y_2(0) = 1 \\ y_3' &= \frac{y_2^2 - y_1 y_3 - 2(De)y_1 y_2 y_3 - M(\gamma - y_2 + (De)y_1 y_3) - \gamma^2}{1 - De y_1^2}; \quad y_3(0) = s_1 \\ y_4' &= y_5; \quad y_4(0) = 0 \\ y_5' &= \frac{y_4 y_2 - y_1 y_5 - 2(De)y_1 y_4 y_2 + M(y_4 - (De)y_1 y_5)}{1 - De y_1^2}; \quad y_5(0) = s_2 \\ y_6' &= y_7; \quad y_6(0) = 1 \\ y_7' &= \frac{-Pr y_1 y_7 - Pr S y_6 - 3(Rd)y_7^2(\theta_w - 1)(1 + (\theta_w - 1)y_6)^2}{1 + Rd(1 + (\theta_w - 1)y_6)^3}; \quad y_7(0) = s_3 \end{aligned} \tag{12}$$

To solve the system (12), guesses for the initial slopes $[f''(0) = s_1, h'(0) = s_2, \theta'(0) = s_3]$ are made and then integration is performed through RK5. The values of these slopes are iteratively estimated through Newton’s method until the far-field conditions $f'(\infty), h(\infty)$ and $\theta(\infty)$ are satisfied. The error tolerance was taken as 10^{-6} , and integrations at different η_{max} were performed in order to ensure that solutions become independent of the domain size.

4 Results and discussion

To validate our findings, we made a comparison of present computational results with those of Abel et al. [3] for a limiting situation (see Table 1). This comparison is found to be very good for all the considered Deborah numbers. Moreover, the results obtained through shooting method are also consistent with those obtained by *bvp4c* of MATLAB.

Figure 1 includes a sample of streamlines at two different values of c . Fig. 2 shows the curves of f' for varying Deborah number De . The results are computed at different values of stretching rates ratio parameter γ , which compares the free stream velocity with the velocity of the stretching surface. We observe that f' is a decreasing function of De when $\gamma < 1$, i.e., when free stream moves slower than the stretching surface. However, when free stream velocity is larger than the stretching velocity ($\gamma > 1$), the velocity field f' appears to increase upon increasing De . Irrespective of the value of parameter γ , the profiles tend to the free stream at shorter distances from the bounding surface, indicating that boundary layer thickness decreases upon increasing the Deborah number De . Deborah number compares the duration of fluid memory (known as fluid relaxation time) to the time of observation. Naturally, the material has a viscous-like response if Deborah number is small, that is, if the relaxation time is

Table 1 Comparison of numerical values of $f''(0)$ with Abel et al. [3] for different values of De with $M = \gamma = 0$

De	Abel et al. [3]	Present results	
		Shooting	<i>bvp4c</i>
0.0	−0.999962	−1.000000	−1.000000
0.2	−1.051948	−1.051890	−1.051889
0.4	−1.101850	−1.101903	−1.101902
0.6	−1.150163	−1.150137	−1.150135
0.8	−1.196692	−1.196711	−1.196711
1.2	−1.285257	−1.285363	−1.285366
1.6	−1.368641	−1.368758	−1.368752
2.0	−1.447617	−1.447650	−1.447648

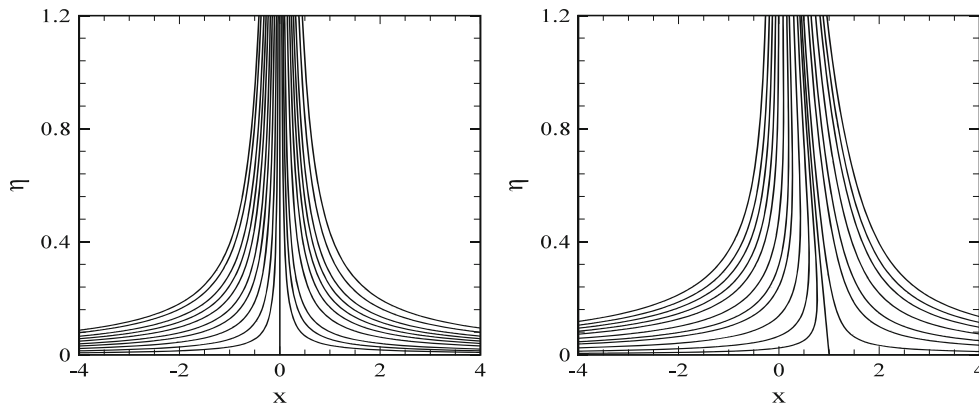


Fig. 1 Streamlines for $De = \gamma = 0.5$ with $c = 0$ (left) and $c = -1$ (right)

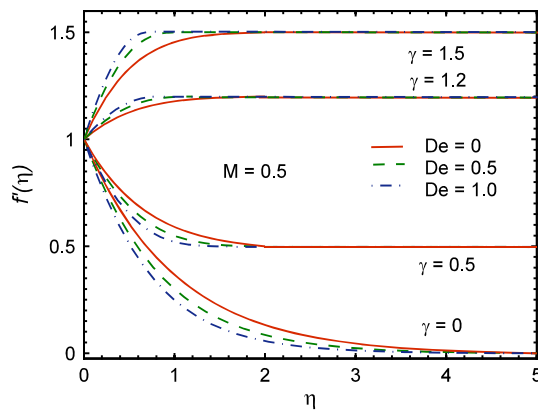


Fig. 2 Profiles of velocity field f' for various values of Deborah number De

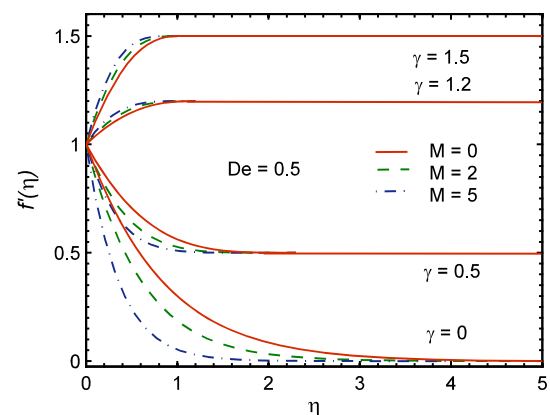


Fig. 3 Profiles of velocity field f' for different values of magnetic field parameter M

small in comparison with the observation time scale. However, when relaxation time is large (or large Deborah number), the elastic effect is dominant compared to viscous effect and the materials response is solid-like.

Figure 3 shows the effects of Hartman number M on the velocity field f' at various values of stretching rates ratio parameter γ . For any value of γ , the profiles are tilted toward the boundary when M is incremented. It means that momentum boundary layer thickness is reduced due to the inclusion of magnetic force term. This opposition to the momentum transport is brought by Lorentz force due to the application of magnetic field.

In Fig. 4, we include the effects of Deborah number De and Hartman number M on the non-alignment function h . We see that magnitude of h reduces upon increasing either the effects of magnetic field strength or the viscoelasticity. Further, the variation in function h with M and De is found to be qualitatively similar for any value of stretching rates ratio parameter γ .

Figure 5 portrays the effects of heat source/sink parameter S on temperature distribution. Naturally, the larger the heat source S , the greater the temperature and the thermal boundary layer thickness. For sufficiently large S ,

fluid temperature becomes greater than that of the bounding surface. As a result, we expect a reverse heat flow between the fluid and the stretching sheet.

The effects of temperature ratio parameter θ_w on temperature θ are depicted in Fig. 6. It is a well-known fact that thermal penetration depth is dependent on the fluid thermal diffusivity. In the current situation, thermal diffusivity has the form $\alpha + 16\sigma^*T^3/3\rho c_p k^*$ as depicted in Eq. (3). This expression gives the sum of classical thermal diffusivity and temperature-dependent term attributed to the radiation effect. Note that the thermal diffusivity is temperature dependent which suggests that thermal boundary layer thickness would vary inside the boundary layer as the temperature changes. Thus, one anticipates that thermal boundary layer thickness will be smaller far from the boundary because free stream temperature is smaller than the wall temperature. As θ_w increases, the second term in the expression of thermal diffusivity increases. This leads to the thickening of thermal boundary layer and, hence, an obvious reduction in wall temperature gradient. Consequently, wall temperature gradient approaches zero value when wall-to-ambient temperature ratio is sufficiently large. Fig. 7 shows that temperature θ increases for increasing values of radiation

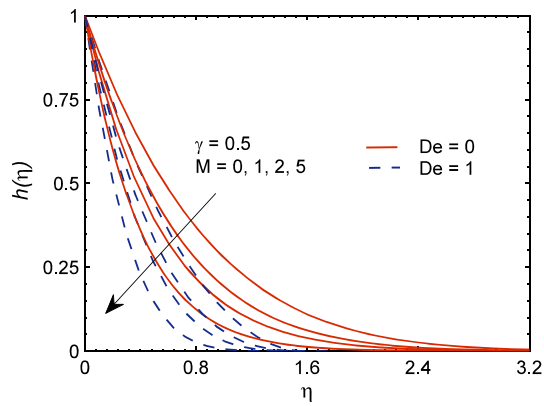


Fig. 4 Effects of Hartman number M and Deborah number De on non-alignment function h

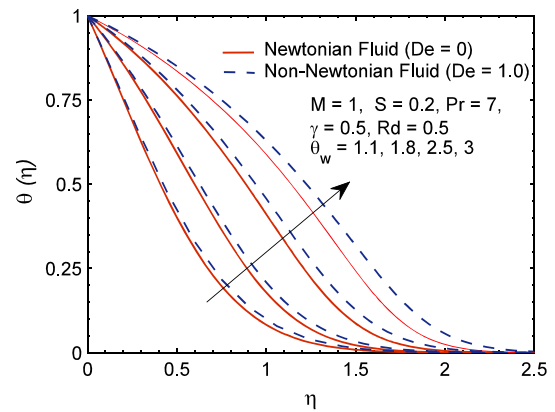


Fig. 6 Temperature profiles for different values of temperature ratio parameter θ_w

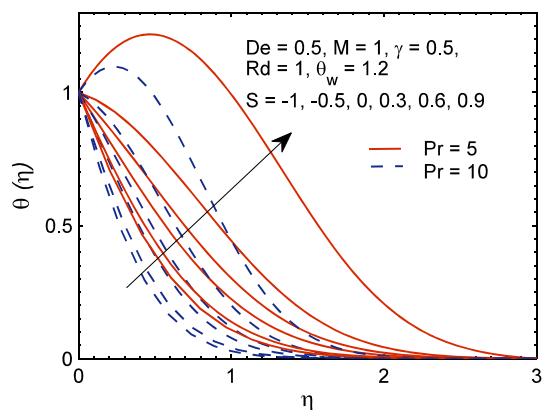


Fig. 5 Temperature profiles for different values of S

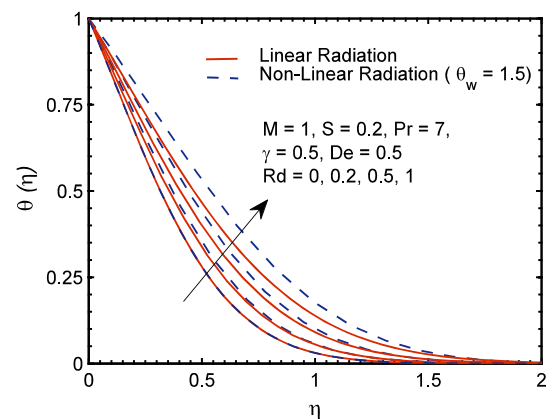


Fig. 7 Temperature profiles for different values of radiation parameter Rd

parameter Rd . Wall temperature gradient $\theta'(0)$ against the temperature ratio parameter θ_w is shown in Fig. 8. We observe that $\theta'(0)$ is inversely proportional to the wall-to-ambient temperature ratio.

Computational results of local Nusselt number $Re_x^{-1/2}Nu_x$ for various parametric values are included in Table 2. It is evident that wall heat flux in viscous fluid is large in comparison with the viscoelastic fluid. Both stretching rates ratio parameter γ and heat source/sink parameter S accelerate the heat transfer from the stretching wall. The value of $Re_x^{-1/2}Nu_x$ is negative when $S = 1$. This is because of the reverse heat flow near the wall as explained earlier through Fig. 4. We also conclude that heat transfer rate decreases upon increasing the magnetic field intensity.

5 Concluding remarks

In this article, we discussed the non-aligned MHD stagnation-point flow of Maxwell fluid bounded by deformable surface. Heat transfer with nonlinear radiation flux and heat

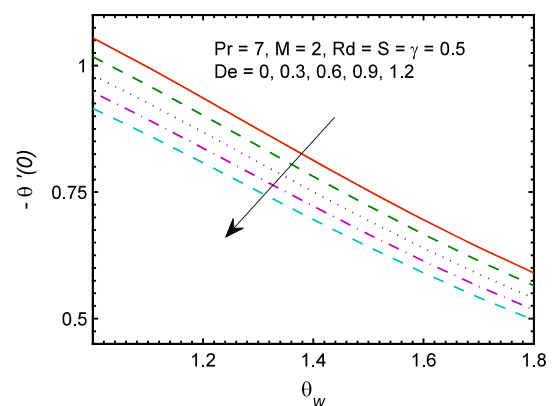


Fig. 8 Effect of Deborah number De on temperature gradient $\theta'(0)$

source/sink is explored. The key aspects of this research are outlined below:

- Hydrodynamic boundary layer becomes thinner when either magnetic field parameter M or Deborah number De is increased.

Table 2 Numerical values of local Nusselt number for different values of γ , S and M with $Pr = 7$, $Rd = 0.5$ and $\theta_w = 1.2$

γ	S	M	Newtonian fluid $De = 0$	Non-Newtonian fluid $De = 0.5$
0	0.5	0	0.748697	0.445486
0.5			1.226268	1.135474
1.5			2.01335	1.924351
0.5	0	1	2.518038	2.47762
	0.5		1.142461	1.046479
	1		-1.899515	-2.504510
	0.5	0	1.226268	1.135474
		2	1.077193	0.976781
		5	-0.939508	-0.833357

- Hydrodynamic boundary layer thickness is a decreasing function of stretching rates ratio parameter γ .
- Thermal boundary layer thickness and heat flux at the surface increase upon increasing the temperature ratio parameter θ_w .
- The effects of all the parameters on the non-alignment function h are qualitatively similar.
- Temperature profiles correspond to the linear radiation case when temperature ratio parameter is sufficiently close to unity.
- Stretching rates ratio parameter γ and heat source/sink parameter S are useful in enhancing the cooling rate of the stretching surface.
- Cooling rate of the sheet is inversely proportional to the viscoelastic fluid parameter.
- To our knowledge, the present work is the first attempt regarding the non-aligned stagnation-point flow of rate-type fluids. In future, possible extension of the present study for unsteady equations can be made. This would be helpful to understand the transition from unsteady flow to the steady-state flow.

References

1. Sadeghy K, Najafi AH, Saffaripour M (2005) Sakiadis flow of an upper-convected Maxwell fluid. *Int J Non-Linear Mech* 40:1220–1228
2. Kumari M, Nath G (2009) Steady mixed convection stagnation-point flow of upper convected Maxwell fluids with magnetic field. *Int J Non-Linear Mech* 44:1048–1055
3. Abel MS, Tawade JV, Nandeppanavar MM (2012) MHD flow and heat transfer for the upper-convected Maxwell fluid over a stretching sheet. *Meccanica* 47:385–393
4. Hayat T, Mustafa M, Shehzad SA, Obaidat S (2012) Melting heat transfer in the stagnation-point flow of an upper-convected Maxwell (UCM) fluid past a stretching sheet. *Int J Numer Methods Fluids* 68:233–243
5. Shateyi S (2013) A new numerical approach to MHD flow of a Maxwell fluid past a vertical stretching sheet in the presence of thermophoresis and chemical reaction. *Bound Value Probl.* doi:10.1186/1687-2770-2013-196
6. Narayana M, Gaikwad SN, Sibanda P, Malge RB (2013) Double diffusive magneto-convection in viscoelastic fluids. *Int J Heat Mass Transf* 67:194–201
7. Khan JA, Mustafa M, Hayat T, Alsaedi A (2015) Numerical study of Cattaneo–Christov heat flux model for viscoelastic flow due to an exponentially stretching surface. *PLoS ONE.* doi:10.1371/journal.pone.0137363
8. Mustafa M, Mushtaq A (2015) Model for natural convective flow of visco-elastic nanofluid past an isothermal vertical plate. *Eur Phys J Plus* 130:1–9
9. Mustafa M, Khan JA, Hayat T, Alsaedi A (2015) Simulations for Maxwell fluid flow past a convectively heated exponentially stretching sheet with nanoparticles. *AIP Adv.* doi:10.1063/1.4916364
10. Khan N, Mahmood T, Sajid M, Hashmi MS (2016) Heat and mass transfer on MHD mixed convection axisymmetric chemically reactive flow of Maxwell fluid driven by exothermal and isothermal stretching disks. *Int J Heat Mass Transf* 92:1090–1105
11. Salahuddin T, Malik MY, Hussain A, Bilal S, Awais M (2016) MHD flow of Cattaneo–Christov heat flux model for Williamson fluid over a stretching sheet with variable thickness: using numerical approach. *J Magn Magn Mater* 401:991–997
12. Mushtaq A, Abbasbandy S, Mustafa M, Hayat T, Alsaedi A (2016) Numerical solution for Sakiadis flow of upper-convected Maxwell fluid using Cattaneo–Christov heat flux model. *AIP Adv.* doi:10.1063/1.4940133
13. Hayat T, Imtiaz M, Alsaedi A, Almezal S (2016) On Cattaneo–Christov heat flux in MHD flow of Oldroyd-B fluid with homogeneous–heterogeneous reactions. *J Magn Magn Mater* 401:296–303
14. Abbasi FM, Shehzad SA, Hayat T, Ahmad B (2016) Doubly stratified mixed convection flow of Maxwell nanofluid with heat generation/absorption. *J Magn Magn Mater* 404:159–165
15. Rahman MM, El-tayeb IA (2013) Radiative heat transfer in a hydromagnetic nanofluid past a non-linear stretching surface with convective boundary condition. *Meccanica* 48:601–615
16. Pantokratoras A, Fang T (2013) Sakiadis flow with nonlinear Rosseland thermal radiation. *Phys Scr* 87:015703
17. Pantokratoras A, Fang T (2014) Blasius flow with non-linear Rosseland thermal radiation. *Meccanica* 49:1539–1545
18. Mushtaq A, Mustafa M, Hayat T, Alsaedi A (2014) Effects of thermal radiation on the stagnation-point flow of upper-convected Maxwell fluid over a stretching sheet. *J Aerosp Eng.* doi:10.1061/(ASCE)AS.1943-5525.0000361
19. Cortell R (2014) Fluid flow and radiative nonlinear heat transfer over a stretching sheet. *J King Saud Univ Sci* 26:161–167
20. Mushtaq A, Mustafa M, Hayat T, Alsaedi A (2014) Nonlinear radiative heat transfer in the flow of nanofluid due to solar energy: a numerical study. *J Taiwan Inst Chem Eng* 45:1176–1183
21. Mustafa M, Mushtaq A, Hayat T, Ahmad B (2014) Nonlinear radiation heat transfer effects in the natural convective boundary layer flow of nanofluid past a vertical plate: a numerical study. *PLoS ONE.* doi:10.1371/journal.pone.0103946
22. Cortell R (2014) MHD (magneto-hydrodynamic) flow and radiative nonlinear heat transfer of a viscoelastic fluid over a stretching sheet with heat generation/absorption. *Energy* 74:896–905
23. Mushtaq A, Mustafa M, Hayat T, Alsaedi A (2014) On the numerical solution of the nonlinear radiation heat transfer problem in a three-dimensional flow. *Z Naturforsch* 69a:705–713

24. Mustafa M, Mushtaq A, Hayat T, Alsaedi A (2015) Radiation effects in three-dimensional flow over a bi-directional exponentially stretching sheet. *J Taiwan Inst Chem Eng* 47:43–49
25. Mushtaq A, Mustafa M, Hayat T, Alsaedi A (2016) A numerical study for three-dimensional viscoelastic flow inspired by non-linear radiative heat flux. *Int J Non-Linear Mech* 76:83–87
26. Kandelousi MS (2014) Effect of spatially variable magnetic field on ferrofluid flow and heat transfer considering constant heat flux boundary condition. *Eur Phys J Plus* 129:248–259
27. Khan JA, Mustafa M, Hayat T, Sheikholeslami M, Alsaedi A (2015) Three-dimensional flow of nanofluid induced by an exponentially stretching sheet: an application to solar energy. *PLoS ONE* 10:e0116603
28. Sheikholeslami M, Ellahi R (2015) Three dimensional mesoscopic simulation of magnetic field effect on natural convection of nanofluid. *Int J Heat Mass Transf* 89:799–808
29. Sheikholeslami M, Abelman S (2015) Two-phase simulation of nanofluid flow and heat transfer in an annulus in the presence of an axial magnetic field. *IEEE Trans Nanotechnol* 14:561–569
30. Sheikholeslami M, Hayat T, Alsaedi A (2016) MHD free convection of Al₂O₃–water nanofluid considering thermal radiation: a numerical study. *Int J Heat Mass Transf* 96:513–524
31. Hosseinzadeh H, Dehghan M, Mirzaei D (2013) The boundary elements method for magneto-hydrodynamic (MHD) channel flows at high Hartmann numbers. *Appl Math Model* 37:2337–2351
32. Dehghan M, Mirzaei D (2009) Meshless local boundary integral equation (LBIE) method for the unsteady magnetohydrodynamic (MHD) flow in rectangular and circular pipes. *Comput Phys Commun* 180:1458–1466
33. Dehghan M, Mirzaei D (2009) Meshless local Petrov–Galerkin (MLPG) method for the unsteady magnetohydrodynamic (MHD) flow through pipe with arbitrary wall conductivity. *Appl Numer Math* 59:1043–1058
34. Dehghan M, Salehi R (2013) A meshfree weak-strong (MWS) form method for the unsteady magnetohydrodynamic (MHD) flow in pipe with arbitrary wall conductivity. *Comput Mech* 52:1445–1462
35. Dehghan M, Mohammadi V (2015) The method of variably scaled radial kernels for solving two-dimensional magnetohydrodynamic (MHD) equations using two discretizations: the Crank–Nicolson scheme and the method of lines (MOL). *Comput Math Appl* 70:2292–2315
36. Pourmehran O, Gorji MR, Ganji DD (2016) Heat transfer and flow analysis of nanofluid flow induced by a stretching sheet in the presence of an external magnetic field. *J Taiwan Inst Chem Eng* 65:162–171
37. Pourmehran O, Gorji MR, Hatami M, Sahebi SAR, Domairry G (2015) Numerical optimization of microchannel heat sink (MCHS) performance cooled by KKL based nanofluids in saturated porous medium. *J Taiwan Inst Chem Eng* 55:49–68
38. Gorji MR, Pourmehrana O, Hatami M, Ganji DD (2015) Statistical optimization of microchannel heat sink (MCHS) geometry cooled by different nanofluids using RSM analysis. *Eur Phys J Plus* 130:1–21
39. Gorji MR, Pourmehrana O, Bandpyb MG, Ganji DD (2016) Unsteady squeezing nanofluid simulation and investigation of its effect on important heat transfer parameters in presence of magnetic field. *J Taiwan Inst Chem Eng* 67:467–475
40. Hamid RA, Nazar R, Pop I (2015) Non-aligned stagnation-point flow of a nanofluid past a permeable stretching/shrinking sheet: Buongiorno’s model. *Sci Rep*. doi:[10.1038/srep14640](https://doi.org/10.1038/srep14640)